Electronic Supplementary Material (ESI) for Journal of Materials Chemistry A

Supporting Information

Surface-Coordination-Induced Selective Synthesis of Cubic and Orthorhombic NaNbO3 and Their Photocatalytic Properties

Authors:
Peng Li[a, b, c], Shuxin Ouyang[b], Yuanjian Zhang[c], Tetsuya Kako[a, b], and Jinhua Ye[*a, b, c, d]

[a]Department of Chemistry, Graduate School of Science, Hokkaido University, Sapporo, Japan
[b]Catalytic Materials Group, Environmental Remediation Materials Unit, National Institute for Materials Science (NIMS), 1-1 Naniki, Tsukuba, Ibaraki 305-0047, Japan
[c]International Center for Materials Nanoarchitectonics (WPI-MANA), National Institute for Materials Science (NIMS), 1-2-1 Sengen, Tsukuba, Ibaraki, Japan
[d]TU-NIMS Joint Research Center, School of Materials Science and Engineering, Tianjin University, 92 Weijin Road, Nankai District, Tiajin, P. R. China

---

[*] Author to whom correspondence should be addressed.

Electronic mail: jinhua.ye@nims.go.jp.

SI-1 Raman spectra of $NaNbO_3$-organic and $NaNbO_3$-inorganic.

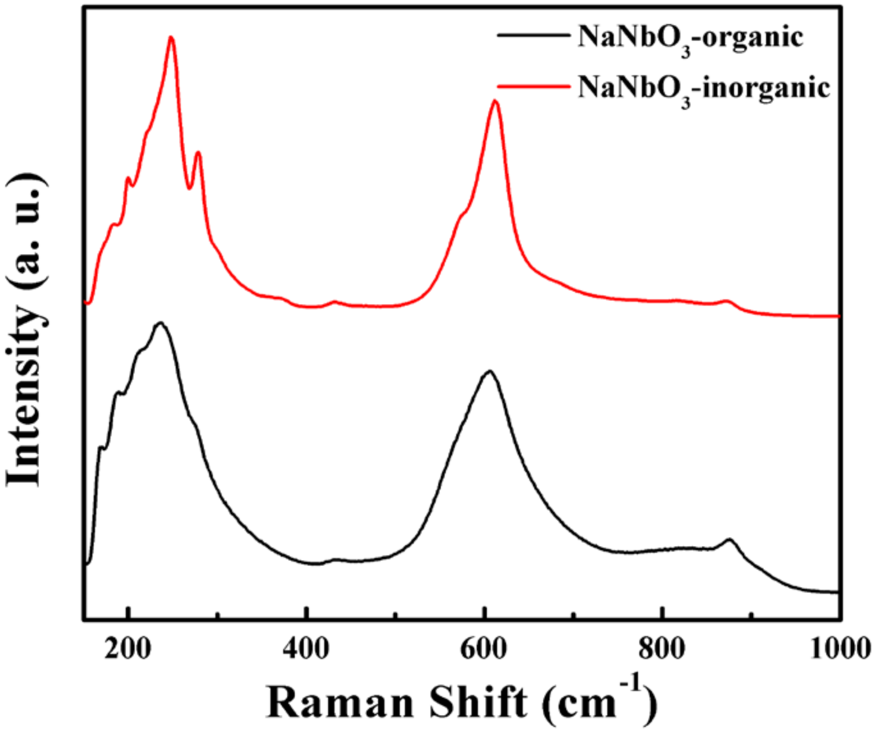

Fig. S1 Raman spectra of $NaNbO_3$-organic and $NaNbO_3$-inorganic.

SI-2 The reference experiment using $^{13}CO_2$ as carbon source in photocatalytic CO_2 reduction over $NaNbO_3$-organic.

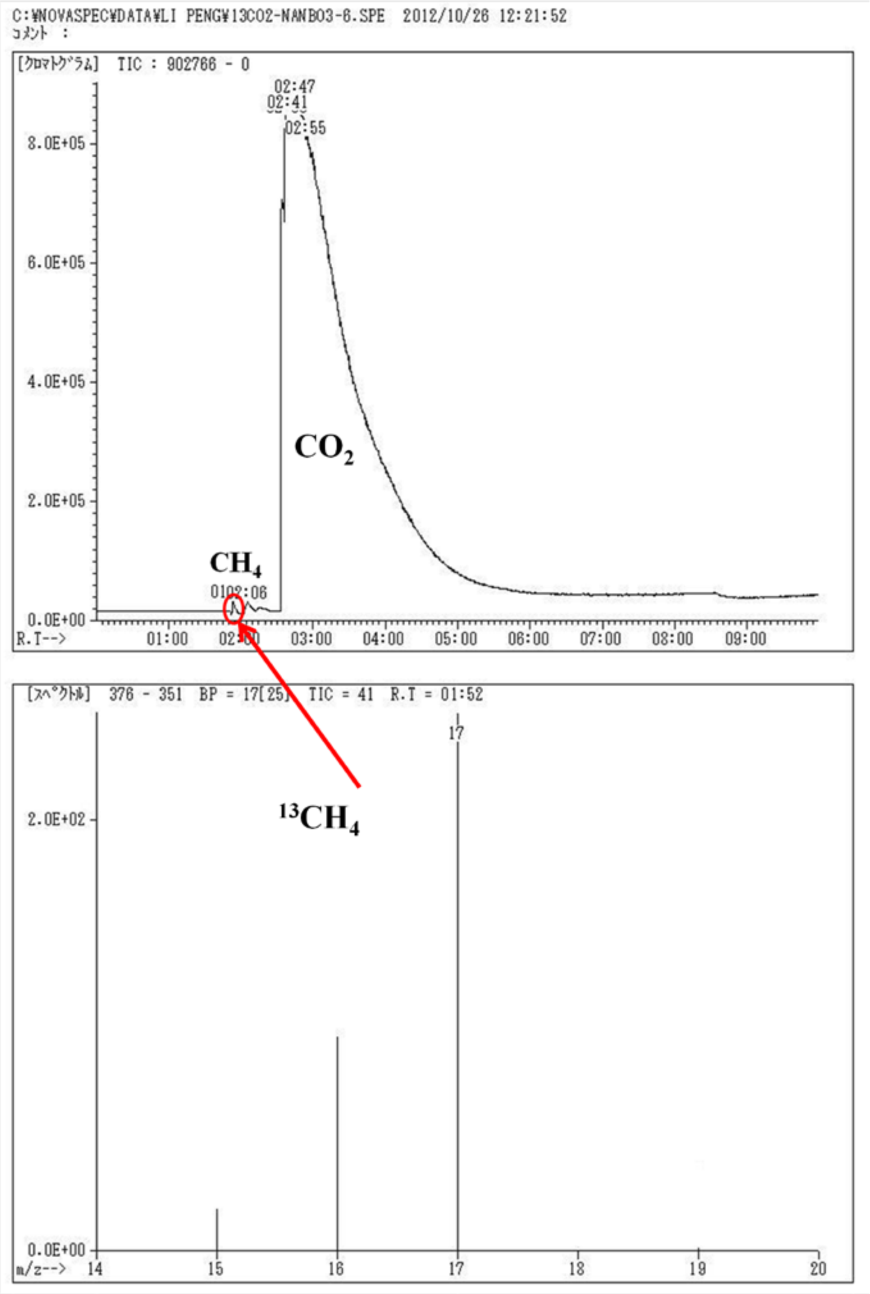

Fig. S2 GC-MS spectra of the products of photocatalytic $^{13}CO_2$ reduction over NaNbO3-organic after 16 h irradiation.

In the GC spectrum, the main peak with the retention time 02:50 is confirmed to be CO_2. Another peak with the retention time 01:52 is the main organic product CH_4. As observed from the mass spectrum, the base peak with m/z of 17 could be determined to be the parent peak (M^+) of $^{13}CH_4$. The peaks with m/z of 16 and 15 could be recognized as the fragment peaks $M\text{-}1^+$ and $M\text{-}2^+$. The intensity ratio of M^+, $M\text{-}1^+$ and $M\text{-}2^+$ matches that of $^{12}CH_4$. Therefore, the main organic product $^{13}CH_4$ is verified to be generated from the reduction of $^{13}CO_2$.

SI-3 The mobility distributions of NaNbO$_3$-inorganic and NaNbO$_3$-organic precursor colloidal particles.

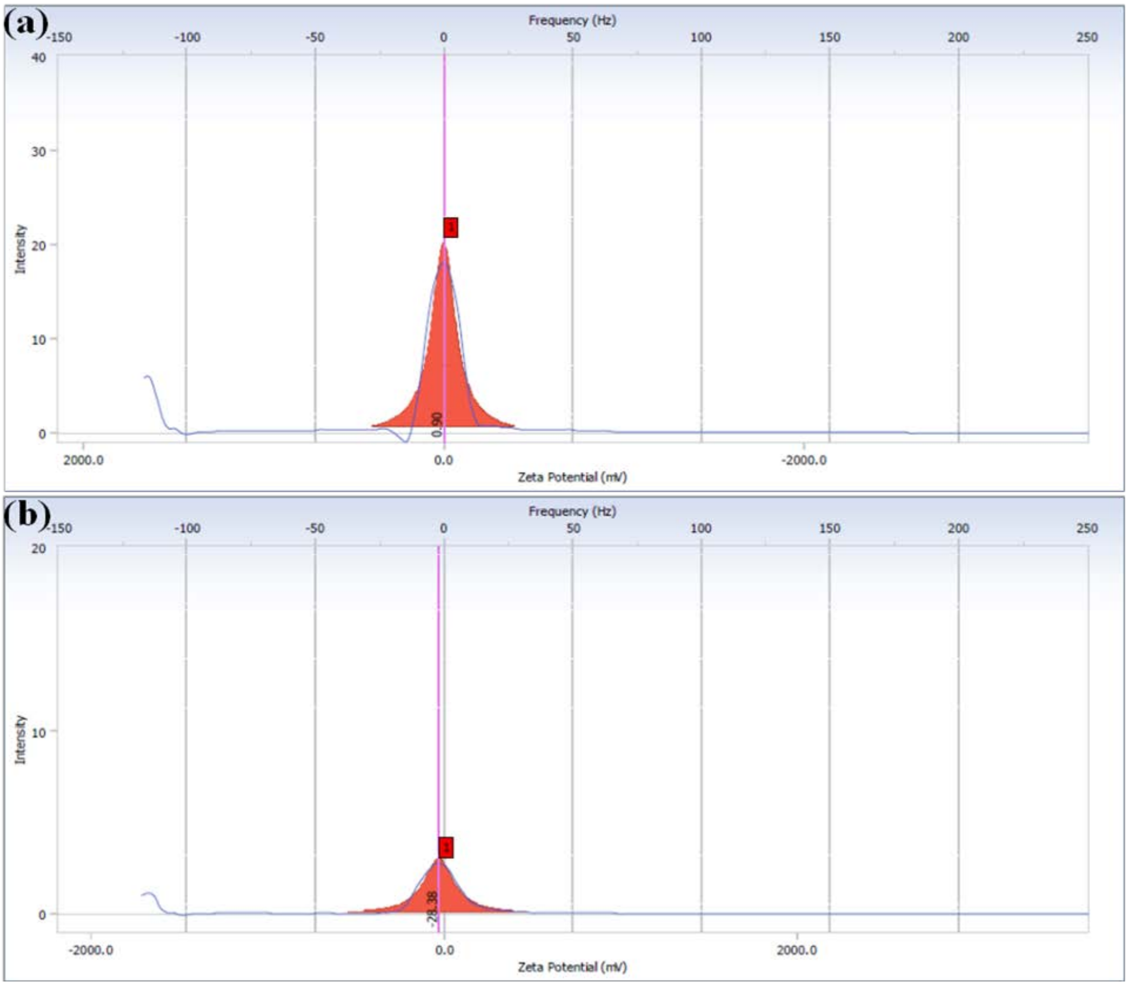

Fig. S3 (a) The mobility distributions of NaNbO3-inorganic precursor colloidal particles. (b) The mobility distributions of NaNbO3-organic precursor colloidal particles.

SI-4 The XRD patterns of the low temperature oxidation samples of $NaNbO_3$-inorganic and $NaNbO_3$-organic.

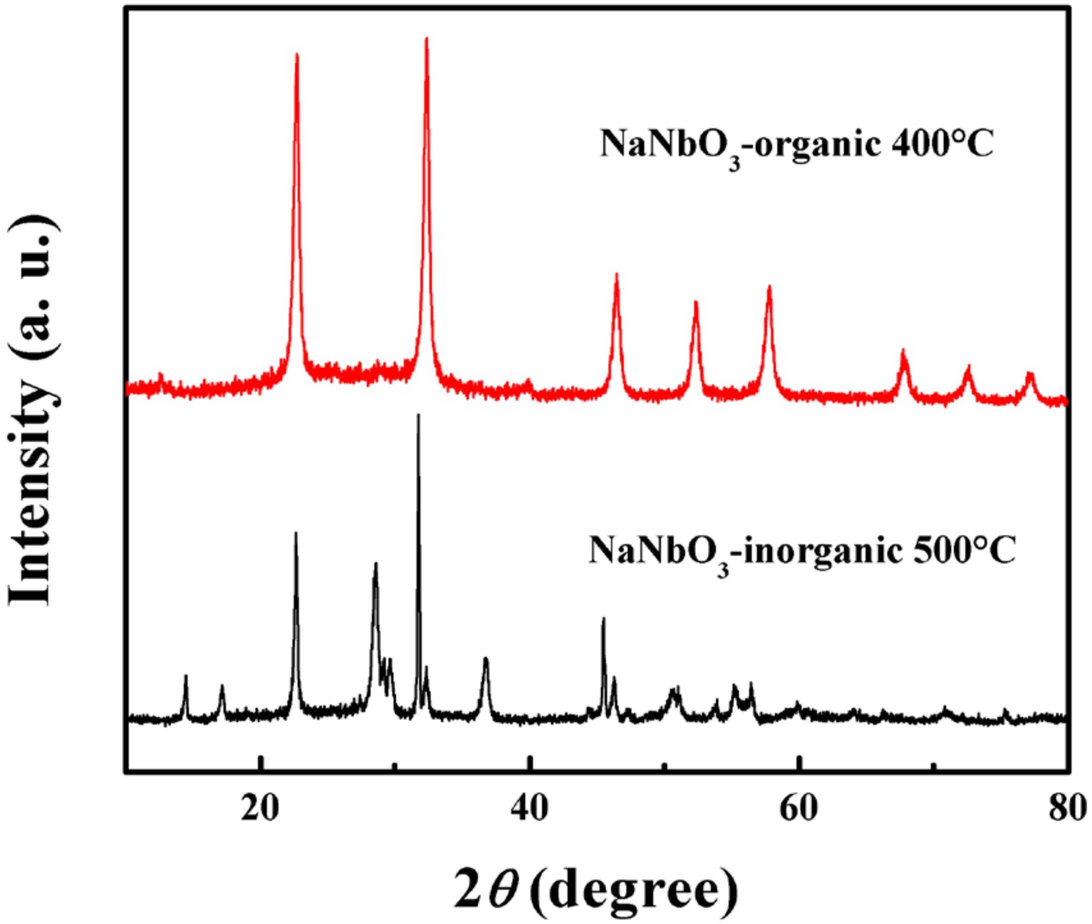

Fig. S4 The XRD patterns of $NaNbO_3$-organic sample oxidized at 400°C and $NaNbO_3$-inorganic sample oxidized at 500°C.

SI-5 TG-DTA plots of the $NaNbO_3$-organic polymer precursor.

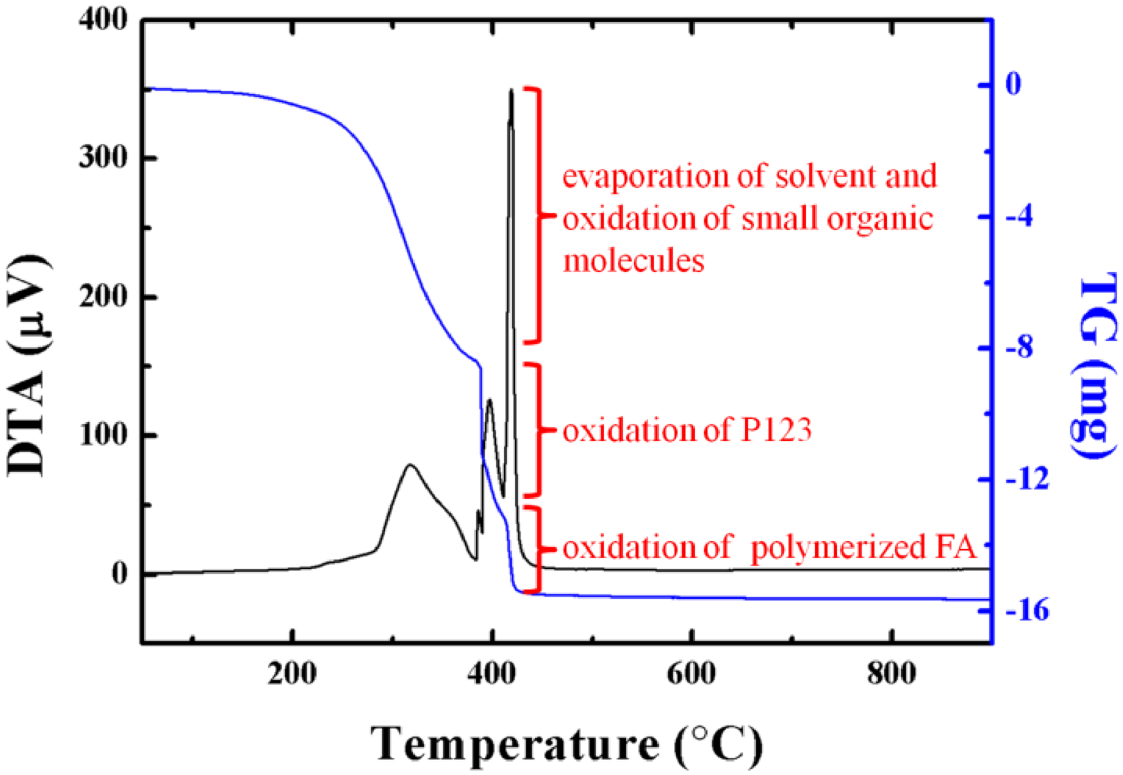

Fig. S5 TG-DTA plots of the $NaNbO_3$-organic polymer precursor.

For the polyfurfuryl alcohol precursor with P123, a subsequent TGA runs in air with a flow rate of 20 mL·min^{-1} shows a significant weight loss that occurs between 200 and 385°C from the evaporation of the remaining solvent and the oxidation of low molecular weight polyfurfuryl alcohol to CO_2. As expected, there is another rapid weight loss between 385 and 415°C from the oxidation of P123. The third weight loss from 415 to 435°C was attributed to the decomposition of high molecular weight polyfurfuryl alcohol.

SI-6 The TEM images of the oxidation temperature relative NaNbO3 samples.

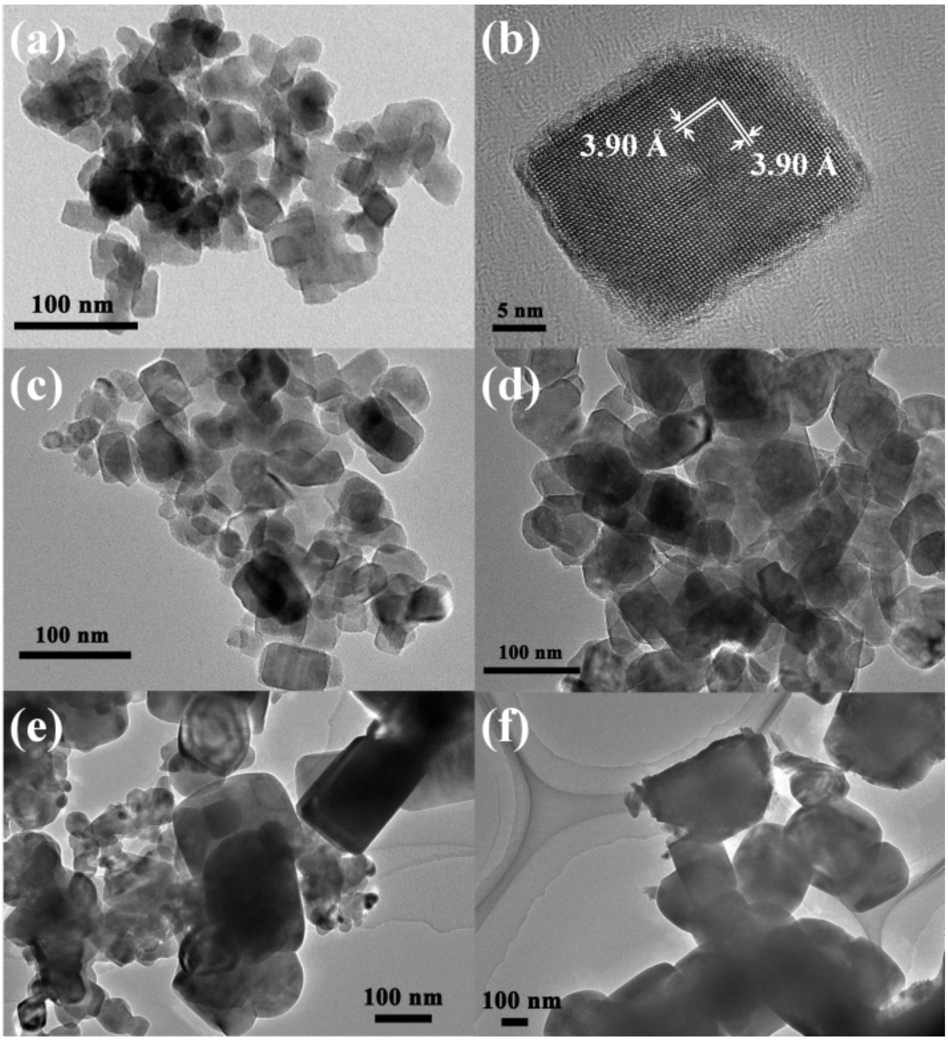

Fig. S6 TEM (a) and HR-TEM (b) images of $NaNbO_3$-500 sample; TEM images of (c) $NaNbO_3$-600, (d) $NaNbO_3$-700, (e) $NaNbO_3$-800, and (f) $NaNbO_3$-900 samples.

When the precursor was oxidized, the particle size has an evident raise along with the evolution of the oxidation temperature. The HR-TEM of $NaNbO_3$-500 gives the clear evidence that, the particle is crystallized in single crystal and exhibits two mutually perpendicular fringes with the same *d*-spacing, 3.90 Å, which could be indexed to the {100} and {010} plane of cubic $NaNbO_3$. From the XRD patterns, the phase transition between the samples oxidized at 600 and 700°C offers a rapid crystal reform and results in a much larger particle size when the sample was annealing at 700°C. In the view of TEM images, the oxidation temperature could affect the crystal growth and a lower oxidation temperature will encourage the smaller $NaNbO_3$ particles. The BET surface areas were measured as 42.1, 27.5, 12.4, 8.9, and 6.8 $m^2 \cdot g^{-1}$ for the samples oxidized from 500 to 900°C, respectively.

SI-7 The FT-IR and UV-Vis absorption spectra of the oxidation temperature relative NaNbO3 samples.

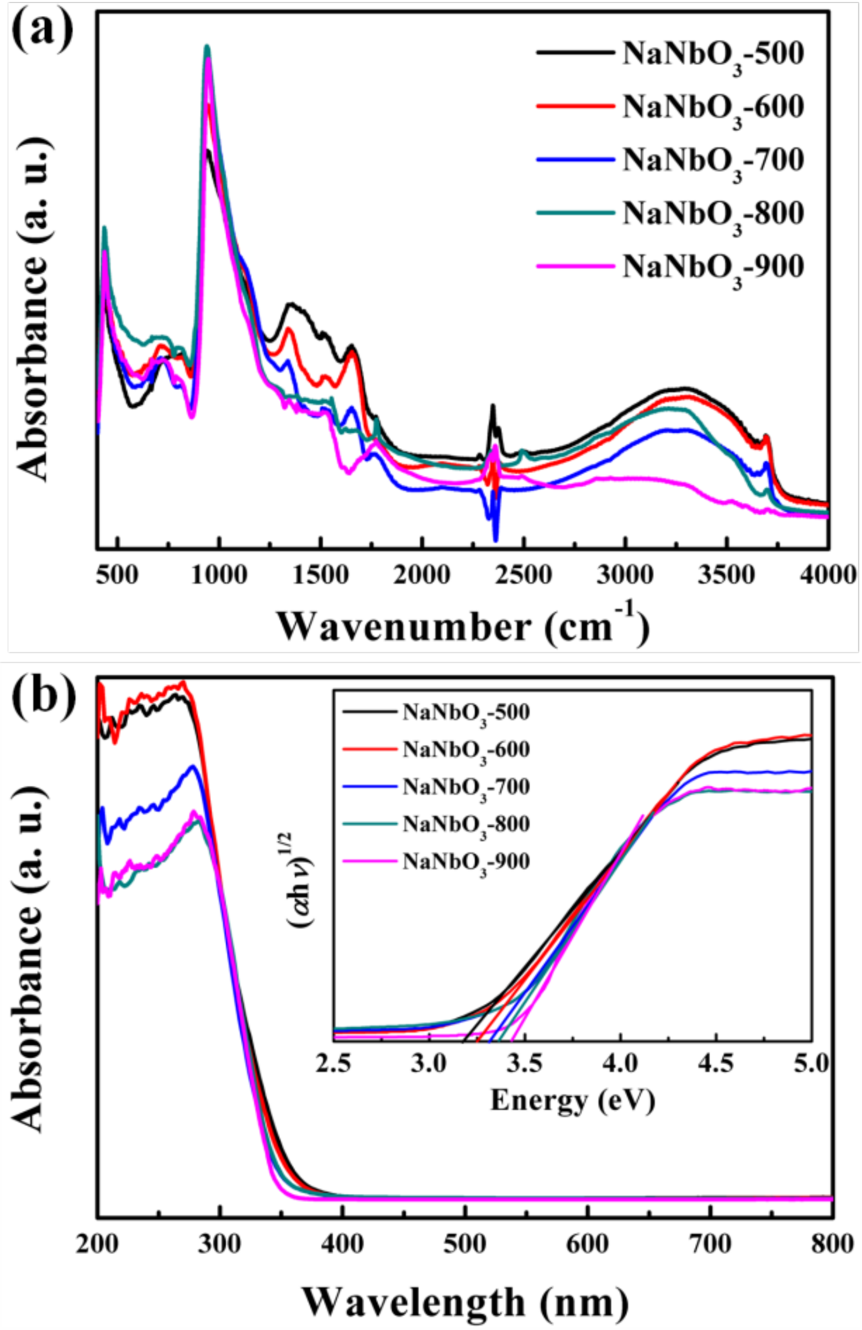

Fig. S7 (a) FT-IR absorption spectra and (b) UV-Vis absorption spectra of the as-prepared oxidation temperature relative $NaNbO_3$ samples. The inset in figure (b) shows the corresponding $(\alpha h\nu)^{1/2}$ ~ $h\nu$ curves.

When the oxidation temperature is changed from 500°C to 600°C, the intensities of these peaks ranging from 1400 to 1700 cm^{-1} which are recognized as the vibrations of C-O bond of carbonate ions decrease. If the temperature continually increases to higher than 700°C, the signals of carbonate ions nearly disappeared. The higher oxidation temperature removed the carbonate ions that are coordinated on the $NaNbO_3$ surface. The decreasing amount of surface carbonate ions induces that the surface energy of $NaNbO_3$ increases and the crystal structure of $NaNbO_3$ reforms from cubic to orthorhombic phase with the annealing energy. UV-visible absorption spectra of the $NaNbO_3$ powder samples oxidized at different temperatures are shown as Fig. S5(b). All the samples have the similar intense absorption with sharp edges in the UV region. From the $(\alpha h\nu)^{1/2}$~Energy plot, the values of the band gaps for as-prepared $NaNbO_3$ samples are determined to be 3.17 3.25 3.32, 3.37 and 3.44 eV, respectively. This band-gap extending from low to high oxidation temperature is consistent with the phase transition from cubic to orthorhombic phase.